Applied Catalysis B: Environmental 96 (2010) 434–440

Contents lists available at ScienceDirect

Applied Catalysis B: Environmental

journal homepage: www.elsevier.com/locate/apcatb

Relation between partial propene oxidation, sulphate content and selective catalytic reduction of NOx by propene on ceria/sulphated titania

Alexandre Baylet[a,b,c,*], Chloé Capdeillayre[a,b,c], Laurence Retailleau[a,b,c], Philippe Vernoux[a,b,c], François Figueras[a,b,c], Anne Giroir-Fendler[a,b,c,**]

[a] Université de Lyon, Lyon F-69003, France
[b] Université Lyon 1, Villeurbanne F-69622, France
[c] CNRS, UMR 5256, Ircelyon, 2 Avenue Albert Einstein, Villeurbanne F-69622, France

ARTICLE INFO

Article history:
Received 17 December 2009
Received in revised form 23 February 2010
Accepted 1 March 2010
Available online 6 March 2010

Keywords:
Selective catalytic reduction
Nitrogen oxide
Nitrogen selectivity
Propene
Ceria
Sulphated titania

ABSTRACT

The propene catalytic oxidation and the selective catalytic reduction of NO by propene (C_3H_6-SCR) have been studied over ceria catalysts supported on sulphated titania (ceria content of 0.9, 0.5, 0.3 and 0.04 wt%). XPS analysis and Raman spectroscopy were carried out in order to obtain information on ceria (oxidation degree, surface content, and particle size) and sulphate compounds (species and surface content). The NOx reactivity was mainly linked to the sulphate content. The higher the sulphate content, the higher the NOx reactivity. The partial C_3H_6 oxidation has a role in the NOx activity. The lower the partial C_3H_6 oxidation into CO, the better the NOx reactivity. However, N_2 selectivity was higher for the sample with the lowest sulphate content (i.e. the highest partial C_3H_6 oxidation). Sulphate compounds like SO_3^{2-} and/or SO_4^{2-} with reduced ceria (Ce^{3+}) activate the C_3H_6 and NO compounds. Moreover, in the range of ceria content studied here, with or without NO in the gas stream, C_3H_6 oxidation was also related to sulphate content and not to ceria content. Nevertheless, the presence of ceria provides oxygen for NO oxidation to form nitrate, oxygen coming from Ce^{3+}Vo species at the surface (Vo: oxygen vacancy). The key parameter between NOx reduction and N_2 selectivity was observed to be the sulphate content.

1. Introduction

Many investigations have been conducted on selective catalytic reduction (SCR) of NO into N_2 by hydrocarbons under lean-burn conditions using non-zeolitic oxide and platinum group metal (PGM) catalysts as a potential process for NOx emission control [1,2]. The HC-SCR mechanism, involving competition between reduction of NOx and reduction of O_2, in lean conditions, is complex and depends on several parameters: (i) the catalyst formulation [3], (ii) the hydrocarbon [4–7] and (iii) the reaction conditions [8]. A number of reviews on HC-SCR have described several possible mechanisms which may occur during the reaction [9–11,1]. Firstly, a simple mechanism for PGM catalysts using a support with low acidity outlines the dissociation of NO on a reduced metal surface to give N_{ad} and O_{ad} followed by desorption of N_2 and N_2O and removal of O_{ad} by the reductant. In the case of PGM catalysts deposited on an acidic support, organo-nitro-type species may contribute to the NOx reduction activity [12]. An acidic support alone has demonstrated that the reduction of NO occurred due to aldehydes; the reaction was fast and selective at low temperatures [13,14]. Secondly, a bifunctional mechanism has been proposed in which hydrocarbons are converted to carbonyl intermediates that react with NOx in an acid-catalysed reaction. The importance of acidity in the reaction has been reported [15–17].

In this work, a tentative of correlation between partial propene oxidation properties, sulphate content and C_3H_6-SCR properties of ceria supported on sulphated titania has been carried out.

2. Experimental part

2.1. Catalyst preparation

The sulphated titania support (theoretical: 2 wt% S) used for catalyst preparation was supplied by Millenium®. Before catalyst preparation, the support was pretreated under air at 500 °C for 2 h. The ceria active phase was deposited at various weight content by impregnation (0.04, 0.3, 0.5, and 0.9 wt%). The ceria acetylacetonate salt precursor ($Ce(C_5H_8O_2)_3$) and the sulphated TiO_2 support were introduced in a 250 mL flask and mixed with 50 mL of distilled water. The solution was stirred for 70 min at 70 °C under atmo-

* Corresponding author at: Université de Lyon, Lyon F-69003, France. Tel.: +33 4 72 43 10 54; fax: +33 4 72 43 16 95.
** Corresponding author at: Université de Lyon, Lyon F-69003, France.
E-mail addresses: alexandre.baylet@ircelyon.univ-lyon1.fr (A. Baylet), anne.giroir-fendler@ircelyon.univ-lyon1.fr (A. Giroir-Fendler).

0926-3373/$ – see front matter © 2010 Elsevier B.V. All rights reserved.
doi:10.1016/j.apcatb.2010.03.001

spheric pressure, then cooled to room temperature under stirring. At the end, the water was evaporated under vacuum at 60 °C in a rotary evaporator. After drying one night under air at 120 °C, the powder was calcined under air at 500 °C for 2 h.

2.2. Characterizations

The quantitative measurement of ceria concentration was performed by ICP-OES using a Horiba Jobin Yvon Activa apparatus. The solid sample was previously dissolved by acid. Specific surface areas (S_{BET}) were estimated from N_2 adsorption at −196 °C (BET method), using a Tristar Surface Area and Porosity Measurement apparatus from Micromeritics. An Axis Ultra DLD from Kratos Analytical spectrometer equipped with a monochromated Al Kα source ($h\nu$ = 1486.6 eV) was used for the surface analysis. A pressure of 10^{-7} Pa was maintained in the chamber during analysis. The analysed area was about (300 μm × 700 μm). Surveys, between 0 and 1200 eV, were obtained with constant pass energy of 150 eV, whereas high resolution spectra were recorded at constant pass energy of 40 eV. Powders were pressed onto small indium foils. Charge neutralization was required for all insulating samples. The peaks were referenced to the $Ti_{2p3/2}$ line at 457.7 ± 0.2 eV, typical for titania powders. Raman measurements were carried out on Horiba Jobin Yvon LabRam HR UV–Vis–NIR spectrometer using green light laser (514 nm). For measurements, the laser was focused on sample analysis area (~1 μm^3). The acquisition time was 20 s.

2.3. NOx reduction reactions

The selective catalytic reduction of NOx by C_3H_6 (C_3H_6-SCR) was carried out in a U-shaped quartz reactor with 200 mg of catalyst. The reactor was electrically heated, with the temperature of the catalyst being monitored using a K-type thermocouple. The reaction mixture was composed of 1100 ppm NO, 1100 ppm C_3H_6 and 9% O_2 in He. The total flow rate was 120 mL min^{-1} which corresponds to a VVH of about 35,000 h^{-1}. Reaction products were analyzed by gas chromatography for N_2, C_3H_6 and CO_2 and by IR–UV for NO, NO_2 and N_2O. The temperature-programmed reaction was started at 25 °C. After stabilization, the catalyst temperature was increased at a rate of 2 °C min^{-1} up to 500 °C. This temperature was maintained 30 min, then decreased to room temperature at a rate of 1 °C min^{-1}. All light-off curves presented in this paper were obtained during the cooling ramp. The conversion of NO into N_2, the N_2 selectivity and the total C_3H_6 conversion were calculated by the following Eqs. (1)–(3):

$$X_{NO-N_2} = 100 \times \frac{2[N_2]_t}{[NO]_{t0}} \quad (1)$$

$$S_{N_2} = 100 \times \left(\frac{2[N_2]_t}{2[N_2]_t + 2[N_2O]_t + [NO_2]_t} \right) \quad (2)$$

$$X_{C_3H_6} = 100 \times \left(1 - \frac{[C_3H_6]_t}{[C_3H_6]_{t0}} \right) \quad (3)$$

2.4. Propene oxidation reactions

Catalytic activity for propene oxidation was measured with a reactant mixture composed of 1100 ppm C_3H_6 and 9% O_2 in He. For each test, 200 mg of catalyst was introduced in a U-shaped quartz reactor. The reactor was electrically heated with the temperature of the catalyst being monitored using a K-type thermocouple. After the reactor was purged under He, a flow rate of 120 mL min^{-1}, corresponding to a VVH of about 35,000 h^{-1}, was passed through the catalyst. After stabilization, the test procedure was started at 25 °C followed by increasing the catalyst temperature, at a rate of 2 °C min^{-1}, up to 500 °C. The temperature was maintained for 30 min and then cooled to room temperature at a rate of 1 °C min^{-1}. The reaction products were analyzed by the same apparatus as those used for the NOx reaction tests. All light-off curves presented in this work were obtained during the cooling ramp. The total C_3H_6 conversion, the conversion of C_3H_6 into CO_2 and CO and the carbon balance are given by the following Eqs. (4)–(7):

$$X_{C_3H_6} = 100 \times \left(1 - \frac{[C_3H_6]_t}{[C_3H_6]_{t0}} \right) \quad (4)$$

$$X_{C_3H_6-CO_2} = 100 \times \left(\frac{(1/3)[CO_2]_t}{[C_3H_6]_{t0}} \right) \quad (5)$$

$$X_{C_3H_6-CO} = 100 \times \left(\frac{(1/3)[CO]_t}{[C_3H_6]_{t0}} \right) \quad (6)$$

$$3[C_3H_6]_{t0} = 3[C_3H_6]_t + [CO_2]_t + [CO]_t \quad (7)$$

For information, the adiabatic temperature due to C_3H_6 oxidation into CO_2 and/or CO is given by Eq. (9). In the case of 100% C_3H_6 converted into CO_2 or into CO, the corresponding maximum ΔT obtained was approximately 64 and 14 °C, respectively.

$$\Delta T = \frac{\Delta Hr(CO_2) \times [C_3H_6]_0 \times X_{C_3H_6/CO_2}}{10^6 \times C_p} + \frac{\Delta Hr(CO) \times [C_3H_6]_0 \times X_{C_3H_6/CO}}{10^6 \times C_p} \quad (9)$$

With ΔHr (C_3H_6 into CO_2) = 1885.5 kJ mol^{-1}; ΔHr (C_3H_6 into CO) = 311.2 kJ mol^{-1}; $[C_3H_6]_0$ = 1100 ppm; 10^6 = ppm and C_p air = 32 J kg^{-1} K^{-1}.

3. Results

3.1. Characterizations

3.1.1. Specific surface area and ceria content

Table 1 summarizes the ceria content of the samples and the S_{BET} of the sulphated TiO_2 support alone and of the catalysts after catalytic testing (previously calcined under dry air at 500 °C for 2 h). The ceria content determined by ICP measurement is close to the theoretical value. Ceria content had only a small impact on the S_{BET} compared to the sulphated titania support with a S_{BET} of 121 m^2 g^{-1}. Furthermore, at the higher the ceria content, the lower the S_{BET} value. The highest S_{BET} obtained was for the Ce0.04 sample at 112 m^2 g^{-1} whereas the lowest S_{BET} value was for the Ce0.9 sample at 106 m^2 g^{-1}. It can be assumed that ceria fills the pores of the sulphated titania support without modifying the pore shape. This was based on the isotherm patterns for the two catalysts which did not display any differences.

3.1.2. Surface composition

XPS analysis was carried out in order to determine the nature of the different compounds (S, C, N, Ti, O and Ce) and to quantify the sulphur element present at the surface of the different catalysts. The general XPS spectra, recorded between 1200 and 0 eV for Ce0.9 sample, is reported in Fig. 1. The binding energy (BE)

Table 1
Specific surface area and Ce content determined by ICP of the Ce/TiO_2 sulphated catalyst.

Catalyst composition	Sample name	Ce content/wt%	S_{BET}/m^2 g^{-1}
TiO_2 sulphated	–	–	121
Ce(0.04%)/TiO_2 sulphated	Ce0.04	0.04	112
Ce(0.3%)/TiO_2 sulphated	Ce0.3	0.30	109
Ce(0.5%)/TiO_2 sulphated	Ce0.5	0.45	107
Ce(0.9%)/TiO_2 sulphated	Ce0.9	0.90	106

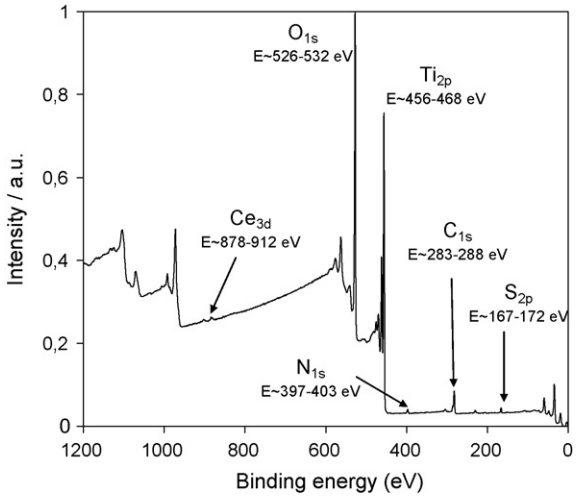

Fig. 1. Overall photoemission spectra for binding energy between 0 and 1200 eV for the Ce0.9 sample.

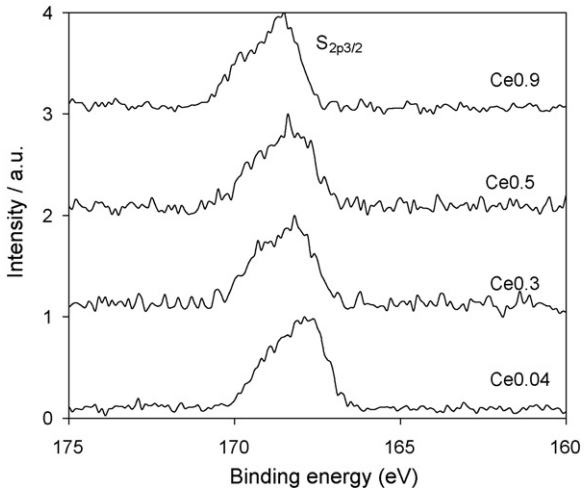

Fig. 2. S(2p) photoemission spectra for Ce catalysts.

ranges for the main peaks of the different elements are 167–172 eV for S_{2p}, 283–288 eV for C_{1s}, 397–403 eV for N_{1s}, 456–468 for Ti_{2p}, 526–532 eV for O_{1s} and 878–912 eV for Ce_{3d}. The positions of the main peaks are given in Table 2. For the C_{1s} band, the peak at 284.6 eV can be ascribed to C graphite (284.3 eV in [18]) and/or C–H bounds (283.9 eV in [19]) and not to interactions between C and Ti (281.6 eV in [20]). Concerning the N_{1s} peak, the value of 399.8 eV is correlated to N_{ads} (399.5 eV in [21]), and not due to bonds between N and Ti (396.8 eV in [22]) or between N and C (395.7 eV in [20]). An enlarged image of the S_{2p} peaks is given in Fig. 2. Concerning the nature of the S species, it was observed that the maximum BE peak of S_{2p}, between 167.6 and 168.4 eV, was linked to sulphate compounds, SO_3^{2-} (166.7 eV in [23]) or SO_4^{2-} (169 eV in [24]), and not due to S from sulphide (S^{2-}) (161.2 eV in [25]) or $S_2O_3^{2-}$ (162.9 eV in [26]). This agrees with the results of Desmartin-Chomel et al. [27] who showed, by FTIR study, that sulphated TiO_2 surface is covered by di-sulphate and/or mono-sulphated species. The di-sulphate species are easily transformed into mono-sulphates by reacting with a strong base like NH_3. Concerning XPS spectra of ceria, the interpretation of the Ce_{3d} peaks is not easy due to the presence of more than 10 peaks correlated to multielectric processes in the Ce^{4+} and Ce^{3+} states [28,29]. Thus, only qualitative analysis on the oxidation of ceria was completed. Due to the low ceria content, Ce peaks could be detected only on the Ce0.9 sample. An enlarged image of the Ce_{3d} peaks is shown in Fig. 3. Firstly, the main $Ce_{3d5/2}$ peak at 880.8 eV is correlated to the Ce_2O_3 compound (881.5 eV in [30]). The BE correlated to the CeO_2 compound is slightly higher, 882 eV [30]. Moreover, Holgado et al. [31] have demonstrated that the ratio between the $Ce_{3d5/2}$ peak at 880.8 eV and its satellite at 883.8 eV could give information on the oxidation state of Ce. They concluded that if the satellite peak height was greater than the main $Ce_{3d5/2}$ peak, then Ce^{3+} is the dominant species in the sample. Secondly, the isolated peak at 916.9 eV was attributed to the presence of Ce^{4+} state and its intensity related to the amount of Ce^{4+} ions. For the Ce0.9 sample, the signal correlating to the u‴ peak (nomenclature of Burroughs et al. [32]) was very low and attributed to the presence of Ce^{3+}. Thus, it was concluded that after (and maybe during) C_3H_6-SCR, the Ce_2O_3 phase is present at the surface of the catalyst and that Ce^{3+}Vo (Vo: oxygen vacancy) defects remain at the surface of the crystallites.

XPS analysis was carried out after ceria impregnation and calcinations to determine the atomic % of the different elements at the surface. The atomic and weight percentages of Ce, Ti and S for the different samples, obtained after reactions, are given in Table 3. Ceria could be detected only on Ce0.9 catalyst, the sample with the highest Ce content. For this catalyst, the experimental weight % of ceria at the surface was 1.1 wt%. This value is close to the overall ceria content determined by ICP analysis, 0.9 wt%. The concentration for S was quantified for all the samples. The S value obtained after ceria impregnation was different from that of the sulphated titania support with a theoretical value of 2 wt% S, and differs between each catalyst. It was observed that ceria impregnation route using aqueous medium and/or calcination treatment modified the stability of the sulphate compound. The Ce0.5 sam-

Table 2
Maximum of the photoemission peaks of O, C, N, Ti, S and Ce elements.

Element	Energy level	Energy binding/eV
O[a]	1s	529.7
C[a]	1s	284.6
N[a]	1s	399.8
Ti[a]	2p3/2	457.7–457.8
	2p1/2	463.5–463.6
S[a]	2p3/2	167.8–168.4
Ce[b]	3d5/2	880.8 satellite 883.8
	3d3/2	899.3 satellite 902
	u‴	916.9

[a] For all catalysts.
[b] Only for Ce0.9 catalyst.

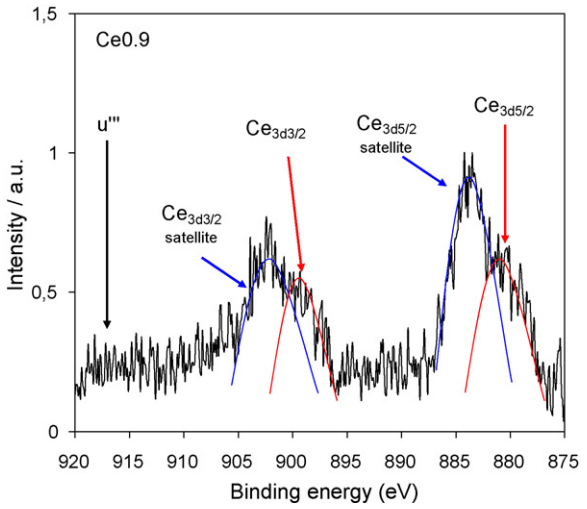

Fig. 3. Zoom of Ce(3d5/2) and Ce(3d3/2) photoemission peak for the Ce0.9 catalyst.

Table 3
Atomic and weight percentage of Ce, Ti and S elements determined by XPS analysis (relative error = ±5%).

Catalysts	Ce	Ti	S	S/Ti [c]
Ce0.04	n.d.[a]	23.7	0.8 ⇔ 1.1	0.03
Ce0.3	n.d.[a]	24.9	1.0 ⇔ 1.4	0.04
Ce0.5	n.d.[a]	23.3	1.6 ⇔ 2.2	0.07
Ce0.9	0.2 ⇔ 1.1[b]	23.5	1.3 ⇔ 1.8	0.06

[a] n.d.: not dertermined.
[b] Atomic % ⇔ weight %.
[c] Atomic ratio.

ple displayed the highest S wt% (2.2). The catalysts ranking in terms of S concentration from highest to lowest is as follows: Ce0.5 > Ce0.9 > Ce0.3 > Ce0.04, corresponding to 2.2, 1.8, 1.4 and 1.1 wt% S, respectively.

3.1.3. Ceria particle size

In order to evaluate the crystal size of the ceria particles, Raman spectroscopy was carried out. The Raman spectra of the different catalysts are reported in Fig. 4. Firstly, the bands located at 152, 404, 527 and 649 cm^{-1} refer to the TiO_2 anatase structure. Lin and Xiaoming showed the same four peaks located at a slightly lower frequency, 147, 397, 515 and 637 cm^{-1} [33]. Intermediate frequencies were obtained by Fang et al. [34]. This frequency shift could be due to the different sample used for calibration, the spectral resolution and the size of the particle: the lower the size, the higher the energy (i.e. nanoparticles shift peaks at low frequency values due to oxygen framework stabilization). Secondly, a band at 462 cm^{-1} was observed only for the Ce0.9 catalyst. It is known that CeO_2 nanoparticles present a strong band at 457 cm^{-1} due to the F_{2g} Raman active mode of the fluorine structure [35]. This band is assigned to ceria particles. This band is characteristic of the CeO_2 mode which is linked to the Ce-O8 vibration (fluorine structure) [36]. For the other experimental catalysts, the ceria content was too low to obtain a Raman signal. Many Raman studies have been done in order to correlate Raman signal and ceria structure. Some authors found relations between the half-width of the Raman peak at 465 cm^{-1} with the ceria particle sizes. The confirmation of the ceria particle sizes was obtained by complementary characterisation methods [37,38]. In this work, the half-width of the peak at 462 cm^{-1} for the Ce0.9 sample was about 24 cm^{-1}. The use of the linear equation obtained by Kosachi et al. [38], H (cm^{-1}) = 10 + 124.7/d (nm), calculates the average value for ceria particle size to be 9 nm. However, when the linear equation of Graham et al. [37], H (cm^{-1}) = 10 + 436/d (Å) was adopted, a lower value, around 2.5 nm was calculated. Both results are in opposition with those obtained by Wang et al. [39]. Indeed, in this study, the presence of small ceria particles (d_p < 17 nm) would involve the apparition in the Raman spectra of two bands located at 270 and 315 cm^{-1}. The Ce0.9 sample did not reveal these bands thus in this last case the ceria particle size should be above 17 nm. Hence, no information could be obtained on the ceria particle size.

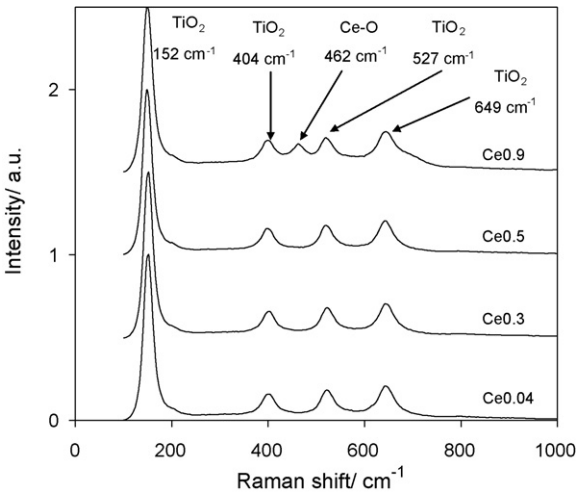

Fig. 4. Raman spectra of the Ce based catalysts.

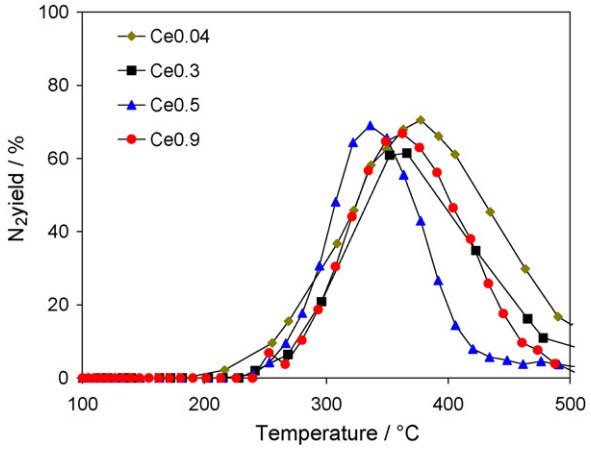

Fig. 5. N_2 yield for Ce catalysts during NOx reduction reaction.

3.1.4. Characterization summary

To conclude on the sample characterization, ceria had a slight inhibitor effect on the surface area and the presence of Ce^{3+} cation was observed on the catalyst surface. The Ce cation species provided sites for oxygen vacancies and the presence of sulphated species such as SO_3^{2-} or SO_4^{2-} anions. However, no clear indication could be obtained on the ceria particle size.

3.2. NO reduction test

In order to evaluate the selective catalytic reduction of NO by C_3H_6 over the ceria/sulphated titania catalysts, NO reduction tests were carried out. In this study, results were focused only on the NO conversion into N_2, N_2 selectivity, and total C_3H_6 conversion. The evolution of NO_2 and N_2O products are not presented here. However, for all the samples, the NO_2 production occurred at temperatures higher than 400 °C and did not exceed 20% at 500 °C (maximum obtained for Ce0.5 sample), whereas N_2O was not detected in the temperature range studied, between 25 and 500 °C. For each experiment the nitrogen balance, including NO, N_2, NO_2 and N_2O, was checked.

Firstly, all the catalysts show a volcano shaped plot for the N_2 yield which tends to decrease to zero at temperatures above 500 °C as reported in Fig. 5. Table 4 summarizes the maximum conversion rate of NO to N_2 and the corresponding temperature. Concerning the maximum conversion, two groups of catalysts can be identified: (i) Ce0.3 sample with a maximum of 61 and (ii) Ce0.04, Ce0.5 and Ce0.9 samples with a maximum of 70, 69 and 67%, respectively. However, even though the profile curves are similar, the Ce0.5 sample displayed the lowest temperature for the maximum conversion, 336 °C. Table 4 presents the maximum N_2 selectivity and the temperature window for a N_2 selectivity of 80%. The variations of N_2 selectivity with the reaction temperature are presented in Fig. 6. Below 335 °C, all the catalysts display the same curve shape, with a fast increase above 200 °C, up to 100%. For temperatures higher than 335 °C, the Ce0.04, Ce0.3 and Ce0.9 samples are more selective towards N_2

Table 4
NOx reduction reaction data for Ce catalysts.

Catalyst	Conversion NO–N_2		N_2 selectivity		Total C_3H_6 conversion		
	Max/%	T_{max}/°C	Max/%	Window T_{80}/°C	$T_{ignition}$/°C	T_{50}/°C	T_{100}/°C
Ce0.04	70	377	100	270–475	216	378	500
Ce0.3	61	367	100	290–447	216	390	500
Ce0.5	69	336	100	280–377	214	310	405
Ce0.9	67	362	100	290–435	226	336	420

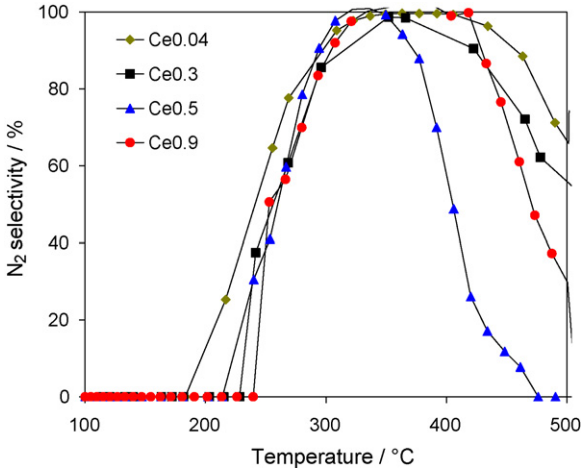

Fig. 6. N_2 selectivity for Ce catalysts during NOx reduction reaction.

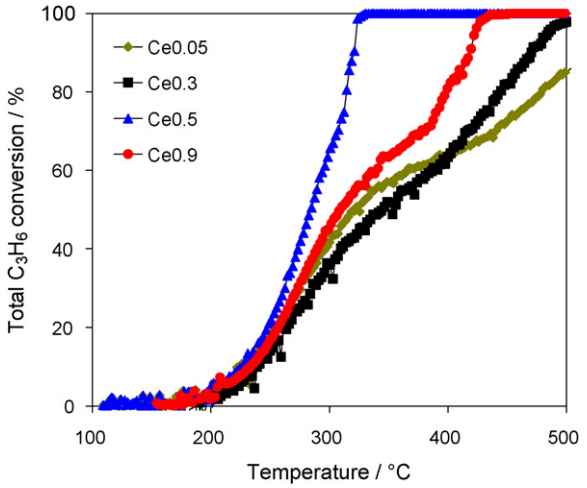

Fig. 8. Total C_3H_6 conversion for Ce catalysts during propene oxidation reaction.

than the Ce0.5 sample. In addition, the N_2 selectivity windows (80%) were larger ($\Delta T > 150$ °C) for Ce0.5 sample ($\Delta T = 100$ °C) than for these last catalysts. The Ce0.5 catalyst had a similar maximum N_2 yield of 69% but it had the lowest N_2 selectivity window.

Finally, the total conversion of C_3H_6 is shown in Fig. 7. Table 4 summarizes the temperature of C_3H_6 ignition and the temperature for 50 and 100% of C_3H_6 conversion. The temperature of ignition was similar for all the catalysts, starting around 220 °C. However, for temperatures higher than 300 °C, the Ce0.5 and Ce0.9 samples were the most active catalysts with a T_{50} of 310 and 336 °C, respectively and both reached a conversion of 100% for C_3H_6 at 410 °C. By contrast, the Ce0.3 and Ce0.04 catalysts presented a T_{50} of 390 and 378 °C, respectively and reached a conversion of 100% at 500 °C.

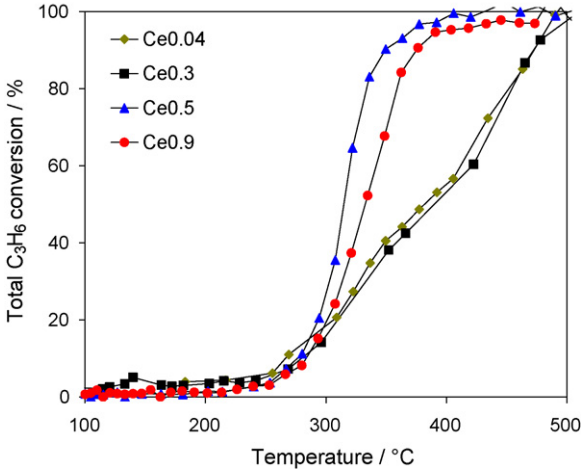

Fig. 7. Total C_3H_6 conversion for Ce catalysts during NOx reduction reaction.

3.3. C_3H_6 oxidation test

The catalytic properties of the ceria/sulphated titania compounds for propene oxidation were evaluated separately. The curves for total C_3H_6 oxidation are presented in Fig. 8. The ignition temperature and the temperature for 50 and 100% conversion of C_3H_6 are given in Table 6. The ceria content did not affect the ignition of propene oxidation. All the catalysts had ignition temperatures around 195 °C. The lowest light-off temperature was obtained for the Ce0.5 sample where T_{50} equalled 284 °C. Ranking the catalyst based on T_{50} order from lowest to highest is as follows: Ce0.5 > Ce0.9 > Ce0.04 > Ce0.3. However, for temperature higher than 400 °C, the conversion order follows the ceria content. The sample with 0.5 wt% of Ce was observed to have the best catalytic behaviour in the propene oxidation reaction.

Arrhenius plots, $\ln(X_{C_3H_6}) = f(1/T)$ for $X_{C_3H_6} < 0.2$, are shown in Fig. 9 and the corresponding values for the activation energy (Ea) are summarized in Table 5. The Ce0.5 sample had the lowest Ea with a value of 60 kJ mol^{-1}. The highest Ea value was obtained for the Ce0.3 sample, 82 kJ mol^{-1}. It is important to notice that for all the ceria catalysts, the analysis of the products during C_3H_6 oxidation revealed only the presence of CO_2 and CO. For Ce0.3 sample, in Fig. 10, the carbon balance evaluated by the sum of ($CO + CO_2$) was equivalent to the total C_3H_6 consumption within experimental error (±5%). For this sample, two reaction pathways can be sug-

Table 5
Activation energy (Ea), $T_{initial}$, T_{50} and T_{100} for total C_3H_6 oxidation of the Ce/TiO_2 sulphated catalyst obtained during propene oxidation reaction.

Catalyst	Ea/kJ mol^{-1}	Total C_3H_6 conversion		
		$T_{ignition}$/°C	T_{50}/°C	T_{100}/°C
Ce0.04	66	190	321	–
Ce0.3	82	200	345	500
Ce0.5	60	193	284	328
Ce0.9	65	194	309	440

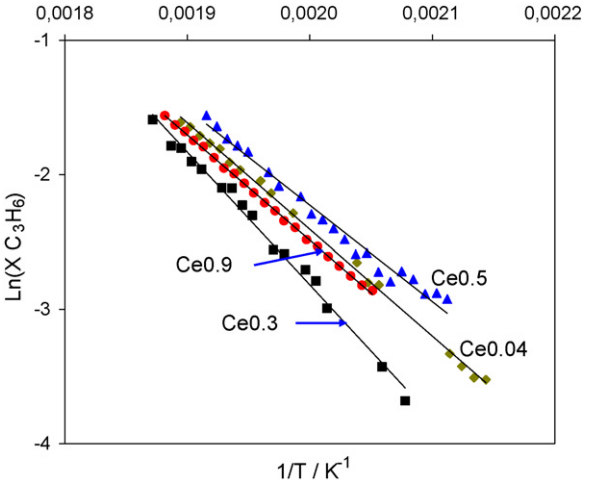

Fig. 9. Arrhenius plot for Ce catalysts obtained after propene oxidation reaction.

gested from this observation. In the first pathway, C_3H_6 is converted to CO, followed by CO oxidation to form CO_2 while in the second pathway, CO and CO_2 are simultaneously produced. For the studied catalysts here, the second pathway was confirmed involving two reaction sites. In the temperature range studied, 100–500 °C, two distinct reaction domains appear. The first reaction domain for Ce0.3 sample is observed in the temperature range of 100–380 °C, while the second reaction domain occurs between 380 and 500 °C. In the first reaction domain, the production of CO and CO_2 increased simultaneously. The partial and total propene oxidation to CO and CO_2 occurred. In the second temperature range, CO conversion decreased while CO_2 production continued to increase. The CO_2 enhancement can be due to the total propene oxidation or the thermal oxidation of CO in the gas phase. However, in order to achieve the simultaneous production of CO and CO_2 two surface reaction sites must be involved. At this stage, it is difficult to characterize such active sites presenting different interactions between ceria, titania, and sulphate compounds.

3.4. Discussion

The C_3H_6-SCR of NO and the C_3H_6 oxidation tests were carried out in order to find a correlation between selective catalytic reduction of NOx, partial C_3H_6 oxidation and sulphate content.

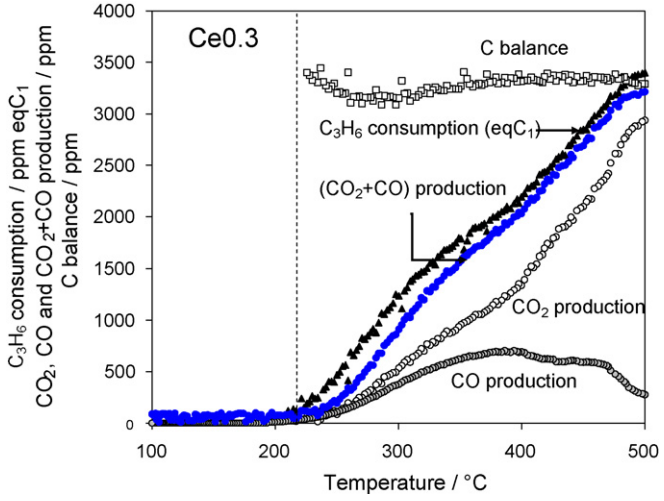

Fig. 10. C_3H_6 consumption, CO_2 and CO production and C balance for Ce0.3 sample during propene oxidation reaction.

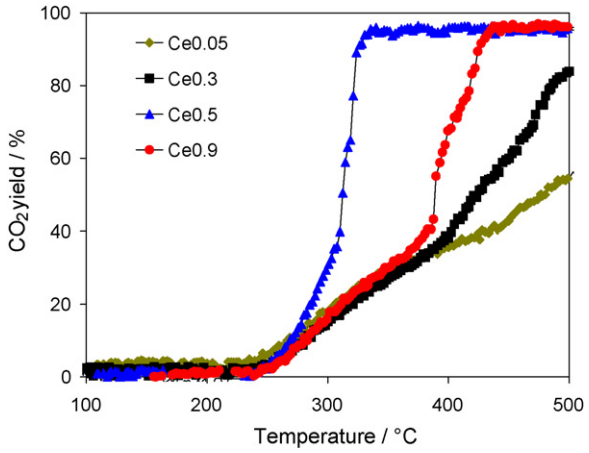

Fig. 11. Conversion of C_3H_6 into CO_2 for Ce catalysts during propene oxidation reaction.

The conversion of C_3H_6 into CO_2 obtained during the C_3H_6 oxidation test is shown in Fig. 11. The ignition temperature and the temperatures where 50 and 100% conversion of C_3H_6 into CO_2 was observed, and the fraction value of propene partially oxidized to CO at 300, 350, 400, 450 and 500 °C are summarized in Table 6. The partial oxidation ratio (R_{PO}) represents the fraction of C_3H_6 oxidised into CO and is defined by the following Eq. (8) and presented in Fig. 12:

$$R_{PO} = 1 - \frac{(n_{C_3H_6/CO_2})_t}{(n_{C_3H_6})_{t0}} = \frac{(n_{C_3H_6/CO})_t}{(n_{C_3H_6})_{t0}} \quad (8)$$

The Ce0.5 sample was observed to have the highest total C_3H_6 conversion to CO_2 (i.e. the lowest CO production). Furthermore, the T_{50} for the Ce0.5 sample was close to 310 °C while the second most active catalyst, Ce0.9, was observed to have T_{50} at 387 °C. The catalyst ranking based on the R_{PO} from lowest to highest is Ce0.04 > Ce0.3 > Ce0.9 > Ce0.5. The same order was observed for N_2 selectivity. However, the inverse order was observed for C_3H_6 oxidation in the absence of NO, C_3H_6 oxidation with NO (C_3H_6-SCR conditions) and NOx activity, Ce0.04 < Ce0.3 < Ce0.9 < Ce0.5. The correlating factor between all these properties seems to be the S wt% content: Ce0.5 > Ce0.9 > Ce0.3 > Ce0.04. Thus, the process occurring during the NOx reduction by C_3H_6 seems to be represented by two main steps: (i) at lower temperatures, ~240 °C, the acidity of the support, due to the presence of S compounds, ini-

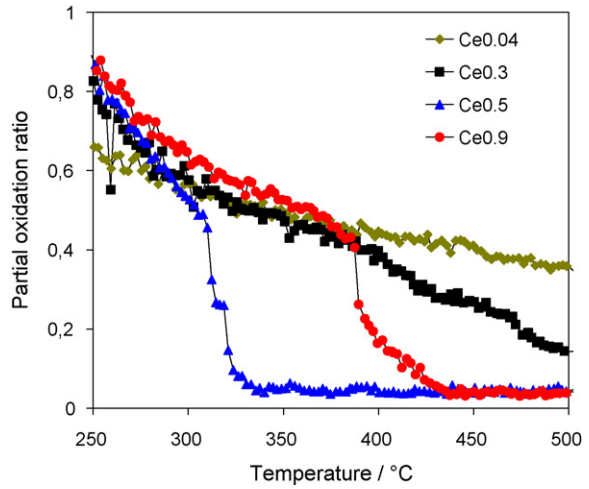

Fig. 12. Partial oxidation ratio of Ce catalysts obtained after propene oxidation reaction.

Table 6
C_3H_6 oxidation reaction data for Ce catalysts.

	Conversion C_3H_6–CO_2				Partial oxidation ratio (R_{OP})				
	$T_{ignition}$/°C	T_{50}/°C	Max/%	T_{max}/°C	300	350	400	450	500
Ce0.04	190	476	54	496	0.57	0.50	0.43	0.40	0.36
Ce0.3	200	424	84	500	0.61	0.47	0.40	0.27	0.14
Ce0.5	193	312	96	335	0.53	0.05			
Ce0.9	194	387	96	434	0.65	0.53	0.16	0.4	

tiates the NOx reduction. The S concentration did not seem to influence the ignition temperature. (ii) At higher temperatures, when the reduction process is ignited, the S wt% has a role on the NOx reduction activity and the higher the S concentration, the higher the CO_2 yield was. This higher total C_3H_6 oxidation into CO_2 decreased the catalyst activity toward N_2 yield, and subsequently, decreased the N_2 selectivity. In the literature, a deeper characterization of the acid-catalyzed process provides a better understanding of the C_3H_6-SCR mechanism over Ce/TiO_2 sulphated catalysts. The mechanism begins in the presence of reduced ceria which provides a surface for the formation of nitrate (NO_3^-) by means of NO^-, N_2O and a dissociation product. However, in parallel, a second minor process could occur where reduced ceria is reoxidized by NO^- formation or NO dissociation, leading to immediate and thermal N_2 desorption [40]. Nitrates can be formed on sulphated TiO_2 surface by the reaction of NO^- on bi- or mono-sulphated species: $NO^- + 2SO_4^{2-} \rightarrow NO_3^- + 2SO_3^{2-}$ and/or $NO^- + SO_4^{2-} \rightarrow NO_2^- + SO_3^{2-}$ [41]. NO^- species are rapidly oxidized and are less stable on sulphated supports than on pure oxides. In the C_3H_6-SCR tests, C_3H_6 reacted with nitrate species to form acetaldehyde intermediate compounds. NO and O_2, from the gas mixture, react quickly with carbonyl compounds to form –CN and –NCO species [17]. As remarked earlier, the partial C_3H_6 oxidation property (R_{PO}) could predict the formation of some intermediate species, like carbonyls (=CO) that are involved in the formation of acetaldehyde (CH_3CHO). NCO is hydrolyzed by water produced in the reaction to form –NH complexes that are then transformed into NH_3 [17]. Finally, a reaction between NH_3 and NO occurs to form N_2. In this bi-functional mechanism, a good activity predictor for N_2 was linked to the number of acid sites, which are the active catalytic sites in C_3H_6-SCR reaction [16,42]. The N_2 selectivity was concluded to be related to the partial C_3H_6 oxidation property (i.e. to the lower wt% S content).

4. Conclusion

In this study, NOx reduction activity evaluated by C_3H_6-SCR over different ceria/sulphated TiO_2 catalysts (ceria content of 0.9, 0.5, 0.3 and 0.04 wt%) was related to the partial C_3H_6 oxidation and the S content. The NOx abatement activity was not correlated to the ceria content, but correlated to the sulphate content. The higher the sulphate content, the higher the NOx activity. Moreover, this activity was linked to the partial C_3H_6 oxidation activity. The lower the partial C_3H_6 oxidation was, the better the NOx activity was. Nevertheless, the N_2 selectivity was better for the catalyst containing the lowest sulphate content (i.e. the best partial C_3H_6 oxidation). Sulphate compounds like SO_3^{2-} and/or SO_4^{2-} and reduced ceria have to activate C_3H_6 and NO compounds. In a second stage, in the range of ceria content studied here, the presence of NO or not, propene oxidation was not linked to ceria content but was related to sulphate content. However, the presence of Ce^{3+}Vo species, involving O vacancies, could provide oxygen for NO oxidation yielding nitrate. To conclude, the sulphate content was observed to be the key parameter in NOx reduction and N_2 selectivity.

Acknowledgments

Thanks are due to the scientific service of IRCELyon for ICP and XPS analyses and Raman measurements.

References

[1] R. Burch, J.P. Breen, F.C. Meunier, Appl. Catal. B 39 (2002) 283–303.
[2] I. Salem, X. Courtois, E.C. Corbos, P. Marecot, D. Duprez, Catal. Commun. 9 (2008) 664–669.
[3] M.D. Amiridis, T. Zhang, R.J. Farrauto, Appl. Catal. B 10 (1996) 203–227.
[4] V. Houel, P. Millington, R. Rajaram, A. Tsolakis, Appl. Catal. B 73 (2007) 203–207.
[5] M.K. Neylon, M.J. Castagnola, N.B. Castagnola, C.L. Marshall, Catal. Today 96 (2004) 53–60.
[6] C. He, M. Paulus, W. Chu, J. Find, J.A. Nickl, K. Köhler, Catal. Today 131 (2008) 305–313.
[7] G. Delahay, E. Ensuque, B. Coq, F. Figuéras, J. Catal. 175 (1998) 7–15.
[8] K.M. Amiridis, J.V. Cavataio, R.H. Hammerle, Appl. Catal. B 10 (1996) 157–181.
[9] A. Fritz, V. Pitchon, Appl. Catal. B 13 (1997) 1–25.
[10] M.D. Amiridis, C. Mihut, M. Maciejewski, A. Baiker, Top. Catal. 28 (2004) 141–150.
[11] R.M. Heck, R.J. Farrauto, Appl. Catal. A 221 (2001) 443–447.
[12] T. Beutel, B. Adelman, W.M.H. Sachtler, Appl. Catal. B 9 (1996) 1–10.
[13] Y.H. Yeom, B. Wen, W.M.H. Sachtler, E. Weitz, J. Phys. Chem. B 108 (2004) 5386–5404.
[14] B. Wen, Y.H. Yeom, E. Weitz, W.M.H. Sachtler, Appl. Catal. B 48 (2004) 125–131.
[15] C.J. Loughran, D.E. Resasco, Appl. Catal. B 7 (1995) 113–126.
[16] F. Figueras, J.L. Flores, G. Delahay, A. Giroir-Fendler, A. Bourane, J.-M. Clacens, A. Desmartin-Chomel, C. Lehaut-Burnouf, J. Catal. 232 (2005) 27–33.
[17] J.L. Flores-Moreno, G. Delahay, F. Figueras, B. Coq, J. Catal. 236 (2005) 292–303.
[18] A. Casagrande, A. Glisenti, E. Lanzoni, E. Tondello, L. Mirenghi, M. Casarin, R. Bertoncello, Surf. Interface Anal. 18 (1992) 525–531.
[19] C. Bichler, H.C. Langowski, M. Bischoff, U. Moosheimer, 39th Annual Technical Conference of the Society of Vacuum Coaters, Philadelphia, 5–10 May, 1996.
[20] P.Y. Jouan, M.C. Peignon, C. Cardinaud, G. Lemperiere, Appl. Surf. Sci. 68 (1993) 595–603.
[21] A. Atrens, A.S. Lim, Appl. Phys. A 51 (1990) 411–418.
[22] M.V. Kuznetsov, J.F. Huravlev, V.A. Gubanov, J. Electron Spectrosc. Relat. Phenom. 58 (1992) 169–176.
[23] R.A. Walton, Coord. Chem. Rev. 31 (1980) 183–220.
[24] P. Marcus, J.M. Grimal, Corros. Sci. 33 (1992) 805–814.
[25] H.W. Nesbitt, I.J. Muir, Geochim. Cosmochim. Acta 58 (21) (1994) 4667–4679.
[26] R.V. Siriwardane, J.M. Cook, J. Colloid Interface Sci. 114 (1986) 525–535.
[27] A. Desmartin-Chomel, J.L. Flores, A. Bourane, J.M. Clacens, F. Figueras, G. Delahay, A. Giroir Fendler, C. Lehaut-Burnouf, J. Phys. Chem. B 110 (2006) 858–863.
[28] J.G. Numan, H. Robota, M. Cohn, S. Bradley, J. Catal. 133 (1992) 309–324.
[29] M. Romeo, K. Bak, J. El Fallah, F. Le Normand, L. Hilaire, Surf. Interface Anal. 20 (1993) 508–512.
[30] T.L. Barr, J. Phys. Chem. 82 (16) (1978) 1801–1810.
[31] J.P. Holgado, R. Alvarez, G. Munuera, Appl. Surf. Sci. 161 (2000) 301–315.
[32] P. Burroughs, A. Hammett, A.F. Orchard, G. Thornton, J. Chem. Soc. Dalton Trans. (1976) 1686–1698.
[33] Y. Lin, Z. Xiaoming, Mater. Lett. 62 (2008) 3764–3766.
[34] J. Fang, X. Bi, D. Si, Z. Jiang, W. Huang, Appl. Surf. Sci. 253 (2007) 8952–8961.
[35] A. Martinez-Arias, M. Fernandez-Garcia, L.N. Salamanca, R.X. Valenzuela, J.C. Conesa, J. Sorya, J. Phys. Chem. B 104 (2000) 4038–4046.
[36] P.S. Anjana, M.T. Sebastian, A.-K. Axelsson, J. Eur. Ceram. Soc. 27 (2007) 3445–3452.
[37] G.W Graham, W.H. Weber, R. Usmen, J. Catal. 130 (1991) 310–313.
[38] I. Kosachi, T. Suzuki, H.U. Anderson, P. Colomban, Solid State Ionics 149 (2002) 99–105.
[39] S. Wang, W. Wang, J. Zuo, Y. Qian, Mater. Chem. Phys. 68 (2001) 246–248.
[40] S.H Overbury, D.R. Mullins, D.R. Huntley, L.J. Kundakovic, J. Catal. 186 (1999) 296–309.
[41] M. Kantcheva, E.Z. Ciftlikli, J. Phys. Chem. B 106 (2002) 3941–3949.
[42] T. Gerlach, U. Illgen, M. Bartoszek, M. Baerns, Appl. Catal. B 22 (1999) 269–278.